Accepted Manuscript

Pivotal role of fluxes in BaTiO3:Eu3+ nano probes for visualization of latent fingerprints on multifaceted substrates and anti-counterfeiting applications

M. Dhanalakshmi, R.B. Basavaraj, G.P. Darshan, S.C. Sharma, H. Nagabhushana

PII: S0026-265X(18)30818-X
DOI: doi:10.1016/j.microc.2018.10.020
Reference: MICROC 3403

To appear in: *Microchemical Journal*

Received date: 2 July 2018
Revised date: 6 October 2018
Accepted date: 7 October 2018

Please cite this article as: M. Dhanalakshmi, R.B. Basavaraj, G.P. Darshan, S.C. Sharma, H. Nagabhushana , Pivotal role of fluxes in BaTiO3:Eu3+ nano probes for visualization of latent fingerprints on multifaceted substrates and anti-counterfeiting applications. Microc (2018), doi:10.1016/j.microc.2018.10.020

Pivotal role of fluxes in $BaTiO_3:Eu^{3+}$ nano probes for visualization of latent fingerprints on multifaceted substrates and anti-counterfeiting applications

M. Dhanalakshmi[1, 2], R.B. Basavaraj[3], G.P. Darshan[4], S.C. Sharma[5], H. Nagabhushana[3, *]

[1]Department of Physics, Govt. Science College, Bangalore-560001, India
[2]Research and Development Centre, Bharathiar University, Coimbatore-641046, India
[3]Prof. C.N.R. Rao Centre for Advanced Materials, Tumakuru University, Tumakuru-572103, India
[4]Department of Physics, Acharya Institute of Graduate Studies, Bangalore-560107, India
[5]Director - National Assessment and Accreditation Council (Work carried out as Honorary Professor, Jain University, Bangalore 560 069, India)

Abstract

In the present work, various fluxes, namely NaCl, NH_4F and NaBr assisted solution combustion route was employed to synthesize novel $BaTiO_3:Eu^{3+}$ (5 mol %) nanophosphors. The influence of the fluxes on structural, morphological and photoluminescence properties of the prepared nanophosphors was investigated in detail. The powdered X-ray diffraction results confirm the cubic structure of the products. The morphological studies reveal that the prepared samples were spherical in shape with agglomeration. The photoluminescence investigation exhibits considerable enhancement in the red emission intensity due to incorporation of fluxes. It was found that, the NH_4F (3 wt %) was considered to be appropriate flux that reduce the forming temperature, improve the morphology and two - fold enhancement in the photoluminescence intensity. The photometric properties of the samples were estimated and were well matched with commercial $BaTiO_3$: Eu^{3+} phosphor. The optimized $BaTiO_3:Eu^{3+}$ (5 mol %), NH_4F (3 wt %) nanophosphors were used as a labeling agent for visualization of latent fingerprints on various porous, semi porous and non-porous surfaces employed by powder dusting method. The visualized fingerprints display highly sensitive, better contrast and small background hindrance. The aforementioned results showcase that the optimized sample was created a new avenue for the facile visualization of latent fingerprints in advanced forensic sciences, anti-counterfeiting and WLED's applications.

Keywords: Solution combustion; Photoluminescence; Photometric properties; Latent fingerprints, Sweat pores.

*Corresponding author: +91- 9945954010, E-mail addresses: bhushanvlc@gmail.com (H. Nagabhushana).

1. Introduction

The morphology of phosphor particles with a homogenous size and shape is an important parameter in next generation displays and solid-state lighting. By dominant these parameters, the potency of devices will greatly be increased. Further, the perfect compactness of the phosphor particles, improves the brightness of displays and lowers production prices. A fluxes are the materials that melts at under the solid state reaction temperature, dissolves one or many constituents and permits material transport to the reaction zone, while not contributing within the solid-state reaction. Preferably, the obtained material ought to be insoluble within the flux. Fluxes don't solely improve the potency of trivalent rare-earth ions (RE), however conjointly play a vital role within the crystal growth. The improved luminescence intensity will be originating from the native crystal field symmetry breaking around RE ions by flux mixing [1-3].

Till date, different routes are used for the preparation of phosphors, like solid-state reaction, co-precipitation, sol-gel, combustion methodology, etc. However, the co-precipitation and sol-gel ways have many demerits because of huge energy loss for the removal of organic components throughout heating procedure and complications in adjusting powder morphology, therefore falling the benefit of industrial production. To mitigate these issues, a flux assisted synthesis methodology was recognized to quicken the kinetics of the development of the preferred products by enhancing diffusion co-efficient. Thus, the flux methodology has potential benefits in particularly bulk production, uniform morphology, regulate the particle size, etc [4-6].

In order to progress the demerits of the above techniques, the flux addition has been advanced in the analysis. Chen et al. confirmed that addition of flux greatly affects the particle

size distribution and growth condition [7]. Cao et al, confirmed by the addition of AlF3 and H3BO3 fluxes of alkali or alkaline earth metals at the same time, increased the particle morphology as well as diminish the calcination temperature [8]. Further, Dai et al. described that without the addition of flux BaF2, the phosphor powder was found to be irregular morphologies with accumulated structure and when the addition of BaF_2 flux, photoluminescence (PL) intensities may be improved [9].

In recent days, lanthanide doped nanophosphors (NPs) are found to be highly advantageous for visualization of latent fingerprints (LFPs) on several complicated surfaces. Owing to its superior emission and functionalities of the NPs that can interrelate with fingerprints (FPs) residues results in better sensitivity, selectivity and low background hindrance in LFPs visualization [10-20]. Uniform and nano sized particles are great impact in order to enhance the adhesion efficiency as well as LFPs visualization over conventionally used micron sized particles. Therefore, lanthanide based NPs were found to be alternative labeling agents in FPs visualization. Further, lanthanide ions (Eu^{3+}, Gd^{3+}, Sm^{3+}) are moderately low toxicity and bio-compatible materials when compared to existing commercially available FP powders, such as bronze, silver, TiO_2, Fe_2O_3, etc. [21].

For the first time, the $BaTiO_3:Eu^{3+}$ (5 mol %) NPs combined with various fluxes (NaCl, NH_4F and NaBr) are prepared by solution combustion (SC) method. The final product was well characterized and used for solid state lighting, advanced forensic and anti-counterfeiting (AC) applications.

2. Experimental

2.1 Synthesis of flux blended $BaTiO_3:Eu^{3+}$ (5 mol %) NPs

The stoichiometric amounts of Barium nitrate [$Ba(NO_3)_2 \cdot 4H_2O$ (Sigma 99.9%)], Europium nitrate [$Eu(NO_3)_3 \cdot 5H_2O$ (Sigma 99.9%)], Tetra butyl titanate [$Ti(C_4H_9O)_4$ (Sigma 99.9%)] and

Aloe Vera (*A. V.*) gel used as a fuel. The basic materials were thoroughly dissolved in double distilled water using a magnetic stirrer for ~ 20-30 min. The reaction solution was placed in a preheated muffle furnace maintained at 450 ± 10 ^{o}C. After ~ 15-20 min, the auto-ignition and metal decomposition was observed. Finally, the obtained powder was annealed at ~700 ^{o}C for ~ 3 h. Similarly, the experiment was repeated using addition of various fluxes, namely NaCl, NaBr and NH_4F in the precursor. The schematic of fabrication procedure of $BaTiO_3$:Eu^{3+} (5 mol %) blended with various fluxes, as shown in Fig.1.

2.2 Visualization of LFPs using optimized $BaTiO_3$:Eu^{3+} (5 mol %), NH_4F (3 wt %) (BENF) NPs

In order to collect the LFPs, the various donor hands were neatly washed using water and soap. Then, the washed fingers were gently pressed with a nominal pressure on various surfaces, namely CD, stainless steel, credit card, SLS glass, aluminium foil, and plastic. The obtained FPs were latent and hence to make them visible, the optimized BENF NPs was stained on the surface with a smooth brushing method using soft feather brush. Finally, the developed LFPs were photographed under 254 nm UV light irradiation.

2.3 Characterization

The Shimadzu made powder X-ray diffractometer with monochromatic CuK_α radiation was used to study structural characteristics of the prepared samples. Morphological (SEM and TEM) analysis was carried out by Hitachi-3000 table top Scanning electron microscope and Hitachi H-8100 provided with a LaB_6 filament equipped with EDS (Kevex sigma TM Quasar, USA). Diffuse reflectance (DR) spectra of all the prepared NPs were recorded by PerkinElmer (Lambda-35) spectrophotometer. PL studies are performed with Horiba (Jobin Yuvon) spectrometer having slit width of 5 nm. The Nikon D3100/AF-S digital camera was used to capture developed LFPs images under normal and 254 nm UV irradiation.

3. Results and Discussion

3.1 Photoluminescence

Fig.2 (a) depicts the PL excitation spectrum of $BaTiO_3:Eu^{3+}$ (5 mol %) NPs. The spectrum display peaks at ~ 380 nm ($^7F_0 \rightarrow {}^5L_7$), 393 nm ($^7F_0 \rightarrow {}^5L_6$), 415 nm ($^7F_0 \rightarrow {}^5D_3$), 462 nm ($^7F_0 \rightarrow {}^5D_2$) and 533 nm ($^7F_0 \rightarrow {}^5D_1$). PLE spectra of $BaTiO_3:Eu^{3+}$ (5 mol %) NPs synthesized by without and with NaCl, NH_4F and NaBr fluxes, as shown in Fig.2 (b). The PLE spectra contain peaks in the range ~ 550 – 750 nm, which were ascribed to $^5D_0 \rightarrow {}^7F_J$ (J = 0, 1, 2, 3 and 4) transitions of Eu^{3+} ions [22-25]. From the figure, it was witnessed that a similar PL profile with maximum intensity was observed in NH_4F blended sample as compared to NaCl and NaBr fluxes (Inset Fig.2 (b)). Hence, it was established that the NH_4F flux was highly suitable for enhancing the pure red color emission without altering the crystal structure and emission profile. The variation in PL emission intensity was probably due to differences in the ionic radius. In addition, the NH_4F flux accelerates the formation kinetics of the NPs by improving the diffusion coefficient as well as sufficient diffusion of atoms. The emission peaks at ~ 592 nm ($^5D_0 \rightarrow {}^7F_1$) and 615 nm ($^5D_0 \rightarrow {}^7F_2$) were due to magnetic dipole (MD) and electric dipole (ED) transitions of Eu^{3+} ions, respectively. Generally, the MD does not govern by the site symmetry of the Eu^{3+} ions in the host lattice, whereas, ED was host dependent and much sensitive. In the present work, ED was dominating over MD, due effective substitution of the Eu^{3+} ions in the crystal sites without an inversion center and low symmetry of the crystal field. Fig. 2 (c) shows the variation of PLE intensity with NH_4F flux concentration (2.5, 5, 7.5, 10 wt %). No peak shift except the change in intensity was noticed. Maximum PL intensity was observed at 7.5 wt % and later intensity diminishes. The diminishing nature was maybe due to the creation of more impurities after the addition of excess NH_4F flux. In order to compare the PLE intensity without and with the

optimized NH_4F flux was studied, as shown in Fig. 2 (d). A 2-fold enhancement in the PL intensity was noticed without altering the emission profile, indicating BENF NPs was suitable for further applications.

In order to explore the possible applications of the prepared NPs in solid state lighting applications, photometric studies, such as International Commission on Illumination (CIE), correlated color temperature (CCT) were evaluated [26, 27]. The estimated values were given in Fig.2 (e & f). It was found that the CIE coordinates were tuned from orange to the pure red region in the optimized sample. The average CCT value (~ 1802 K) was well within the acceptable range (< 5000 K). Generally, the color purity is a major tool in order to assessing the significance of the phosphors. Hence, the color purity of the prepared NPs was estimated by using the following equation;

$$color\ \ purity = \frac{\sqrt{(x_s - x_i)^2 + (y_s - y_i)^2}}{\sqrt{(x_d - x_i)^2 + (y_d - y_i)^2}} \times 100\% \quad \text{---------- (1)}$$

where, (x_s, y_s), (x_i, y_i) and (x_d, y_d); color co-ordinates of the light source, CIE illuminant and dominant wavelength of light source, respectively. In the present case, the color purity of the optimized sample was found to be ~ 92 %. Hence, the optimized NPs finds potential applications in the production of WLEDs as a red phosphor.

3.2 Judd–Ofelt analysis

The Judd–Ofelt (J-O) intensity parameters (Ω_2 and Ω_4) as well as other radiative properties, such as transition probabilities, radiative life time, branching ratio, asymmetric ratio, stimulated emission cross-section quantum efficiency were estimated based on the relations given in the literature [28, 29]. The estimated values were given in Table 1. Normally, the Ω_2 parameter was highly sensitive to the ligand environment as well as depending on the covalence between dopant

ions and ligands anions. It was witnessed from the table that the value of Ω_2 was minimum in BENF NPs suggesting that the enhancement in the symmetric nature of the Eu^{3+} ions in $BaTiO_3$ NPs. Further, the diminution in the Ω_4 values with fluxes was also observed, which indicating that the efficiency for the $^5D_0 \rightarrow {}^7F_2$ (612 nm) transition enhances. The radiative lifetime, transition probability, branching ratio and emission peak cross-section were calculated and tabulated Table 1. It was evident that, the higher values of emission peak cross-section and branching ratio suggests that the optimized BENF NPs has a potential application for lasing action and therefore it, was highly useful for red laser application.

4. Visualization of LFPs by powder dusting method

In order to accomplish the sensitivity and selectivity of the prepared product, the various fluxes assisted NPs on aluminum foil surface were stained on LFPs via powder dusting method and photo captured under UV 254 nm light (Fig.3). Well-defined ridge characteristics were observed in NH_4F flux blended samples as compared with the other images (Fig.3 (c)). Fig.4 shows the FPs visualized by the optimized NPs on various non-porous surfaces (highlighter pen, metal scale, granite, metal punch pad, stapler) under 254 nm UV light. A clear ridge patterns including level 1 and 2 were undoubtedly visualized under 254 nm UV light, due to its nano-regime and better adhesive nature. The LFPs visualized by dusting BENF NPs on various porous magazine covers with different backgrounds, aluminium foil, playing card, white paper and paper coffee cup, as shown in Fig.5. The results clearly demonstrated that, the LFP visualized by optimised NPs fluorescent reveal unique and sharp ridge details without any background interference.

Generally, LFPs are categorized into three different levels, namely level 1, level 2 and level 3 details. Among, the level 1 details, namely delta, loop and whorl are unclear and not enough for personal identification. Further, Level 2 details consists of various minutiae, such as

bifurcation, cross over, lake, hook, short ridge, island, etc., which are clear and distinctive. However, level 3 details are encompassing sweat pores, small deviations in ridge track and edge contours, which are more evidential details in order to encounter the individualization in advanced forensic science. In our work, we established the LFPs visualization on glass using the optimized BENF NPs under UV 254 nm light, as shown in Fig.6 (a). It was evident from the figure that, the afore-mentioned all the three levels ridge details in FPs are clearly identified. The obtained results are considered as extremely vital quantitative data to identify individuals. The pixel profile of FP part was depicted in Fig. 6 (b). Through the pixel profile, ridges (cyan color) and furrows (black color) pattern are distinguished in the FPs. Further, FP images of four different donors on aluminum foil surface stained by optimized BENF NPs under UV 254 nm light, as shown in Fig.7. It was clearly evident from the figure that each individuals having a unique FP patterns namely central whorl, ulnar arch, plain arch and pocket whorl. In addition, to authenticate the quality of the FPs images visualized using BENF NPs, some conventional commercial powders, namely Fe_2O_3 and TiO_2 were selected as control (Fig.8). As can be seen from the figures, the LFPs visualized by using commercial powders showed poor image quality with few minutiae details. However, the BENF NPs stained FPs exhibit best image quality with defined ridge minutiae. Hence, the obtained results further demonstrated the significance of the BENF NPs in the advanced forensic sciences.

In recent years, the variety of AC tools, namely simple marker, plasmonic security labels, holograms, security inks, etc. were used to safeguard against forging [30, 31]. Many attempts were made on luminescent based security inks, namely CdS, CdSe, CdTe, etc., but they suffer from some serious issues, such as toxicity, broad emission, and hazardous to user. However, in order to enhance the security features, rare earth doped NPs offer innovative security tool owing

to distinctive physical, chemical, optical properties, etc. Therefore, RE doped NPs based transparent security ink have considered to be a real alternative for AC applications. Keeping in this in mind, we developed AC tags using optimized BENF NPs assisted ink followed by dip pen mode. The digital photographs of various handwritten AC tags under normal and UV 254 nm light illumination, as shown in Fig.9. The obtained result evident that, the AC tags exhibit enhanced red emission under UV 254 nm light illumination.

5. Structural analysis

The powdered X-ray diffraction (PXRD) profiles of the prepared samples was depicted in Fig.10 (a). The obtained profiles confirm the existence of the single cubic phase. The results were well matched with a standard JCPDS No. 74-1961 [32]. Small shift in the peak (110) towards lower angle side with increase of flux weight percentage was observed (Fig.10 (b)). No impurity and dopant peaks were observed, signifying that the dopant Eu^{3+} ions were effectively substituted in the host site. Broadening in the PXRD peaks was used to calculate average crystallite size (D) by employing Scherrer's relation given in the literature [33]. The estimated values of D were found to be ~ 25 – 35 nm.

5.1 DR studies

DR spectra of the $BaTiO_3$:Eu^{3+} (5 mol %) and BENF NPs, as shown in Fig.10 (c). The spectra exhibit peaks at ~ 395, 405, 460, 582 nm, which were attributed to $^7F_0 \rightarrow {}^5D_4$, $^7F_0 \rightarrow {}^5L_6$, $^7F_0 \rightarrow {}^5D_2$, $^7F_0 \rightarrow {}^5D_0$ transitions of Eu^{3+} ions, respectively. In addition, weak absorption peaks observed in the shorter wavelength range was may owing to the formation of meta-stable states in between valence and conduction band by the Eu^{3+} ions. Further, the DR spectra was utilized to estimate the energy band gap (E_g) of the samples by employing Kubelka–Munk (K-M) theory as given in the literature [34]. The E_g values were estimated by plotting $[F(R)]^2$ versus photon energy

($h\nu$), as depicted in inset Fig.10 (c). The calculated value of E_g was found to be ~ 3.32 and 3.39 eV. The small changes in the E_g values was observed, which may be due to minor structural variations in the host [35, 36].

5.2 Morphological analysis

Fig.11 (a-d) depicts SEM micrographs of $BaTiO_3:Eu^{3+}$ (5 mol %) NPs with and without fluxes. It can be evident from the figure that, sample exhibits large number of uneven and irregular shaped particles were observed in the absence of the flux. However, flakes, spherical and non-uniform agglomerated particles evidenced in the presence of fluxes. SEM images of BENF samples exhibit spherical shape particles and it was one of the important key factor in order to enhance the luminescence efficiency. The spherical morphology was achieved by the formation of liquid via the melted flux, which may have increased the surface tension during reaction process, making particles coagulate together. This melt flux enhanced the slide and rotation of particles. This effect promoted the particle-particle contact and particle growth and hence increased the particle size [37]. The melted flux also increased the mobility and homogeneity of solid reactants significantly during synthesis. These phenomena are considered to be most important for eliminating the surface defects of the phosphors and improving the PL intensity [38]. In addition, SEM images of various concentrations of NH_4F (2.5 – 10 wt %) assisted samples, as shown in Fig.11 (e-h). When lower weight percent of NH_4F (2.5 wt %) flux, irregular with closely stacked spherical particles were observed (Fig.11 (e)). However, with increase of flux concentration from 5 – 10 wt %, the uniform spherical shaped particles were obtained (Fig.11 (f-h)).

Fig.12 (a-d) depicts TEM images of with and without flux assisted NPs. As can be seen from the images that the irregular shaped particles were observed in the absence of flux. However, TEM images in the presence of fluxes (Fig.12 (b-d)) were agreement with the

corresponding SEM results. Fig.12 (e & f) depict the HRTEM image and SAED pattern of the optimized BENF NPs. From HRTEM, the inter-planar spacing (d) resultant from the (110) plane was estimated and obtained to be ~ 0.28 nm. The well crystallinity of the prepared sample was confirmed in the SAED profile and obtained rings are good agreement with the (hkl) planes.

Conclusions

Various fluxes blended red light emitting $BaTiO_3:Eu^{3+}$ (5 mol %) NPs have been prepared via SC route. The XRD patterns confirm the pure cubic phase of the samples. The PL studies exhibit characteristics emission peaks at ~ 592, 615, 654 and 702 nm attributed to $^5D_0 \rightarrow {}^7F_J$ (J = 0, 1, 2 and 3) transitions of Eu^{3+} ions, respectively under NUV excitation. It was witnessed that a similar PL profile with maximum intensity was observed in NH_4F blended sample as compared to NaCl and NaBr fluxes assisted samples. A 2-fold enhancement in the PL intensity was noticed without altering the emission profile, indicating NH_4F blended sample was suitable for further applications. The calculated CIE coordinates for the optimized phosphor is found to be (0.65, 0.35) under NUV excitation, which are close to the coordinates of NTSC standard for red color. The optimized BENF NPs was used as a labeling agent for visualization of LFPs on various porous, semi porous and non-porous surfaces employed by powder dusting method. The visualized LFPs reveals various ridge details, namely sweat pores, eye, island, ridge end, specialty, bifurcation and scar with high sensitivity, selectively, contrast and low background hindrance. Therefore, the optimized sample was considered to be novel material for WLED's, forensic science and anti-counterfeiting applications.

References

1. R.B. Basavaraj, H. Nagabhushana, B. Daruka Prasad, G.R. Vijayakumar, Zinc silicates with tunable morphology by surfactant assisted sonochemical route suitable for NUV excitable white light emitting diodes, Ultrason. Sonochem., 34 (2017) 700.
2. G. Swati, S. Bishnoi, P. Singh, B. Rajesh, G. Kumar, P. Seth, D. Haranath, Novel flux-assisted synthesis for enhanced afterglow properties of (Ca,Zn)TiO_3:Pr^{3+} phosphor. J. Alloys Compd., 698 (2017) 930.
3. Z. Jiang, J. Gou, Y. Min, C. Huang, W. Lv, X. Yu, X. Su, L. Duan, Crystal structure and luminescence properties of a novel non-rare-earth activated blue-emitting garnet phosphor $Ca_4ZrGe_3O_{12}$: Bi^{3+} for n-UV pumped light-emitting diodes. J. Alloys Compd., 727 (2017) 63.
4. S. Yang, G. Xiao, D. Ding, Y. Ren, L. Lv, P. Yang, J. Gao, Solid-phase combustion synthesis of calcium aluminate with $CaAl_2O_4$ nanofiber structures, Ceram. Int., 44 (2018) 6186.
5. Subhash Sharma, Vikash Singh, R. K. Dwivedi, Electrical properties of (1−x) BFO – (x) PZT multiferroics synthesized by sol-gel method: Transition from relaxor to non-relaxor, J. Alloys Compd., 682 (2016) 723.
6. Subhash Sharma, J. M. Siqueiros, Gunjan Srinet, Shiv Kumar, Brijmohan Prajapati, R. K. Dwivedi, Structural, electrical, optical and dielectric properties of sol-gel derived (1 − x) $BiFeO_3$ – (x) $Pb(Zr_{0.52}Ti_{0.48})O_3$ novel multiferroics materials, J. Alloys Compd., 732 (2018) 666.
7. D. Chen, Y. Zhou, W. Xu, J. Zhong, Z. Jia, W. Xiang, Enhanced luminescence of Mn^{4+}:$Y_3Al_5O_{12}$ red phosphor via impurity doping. J. Mater. Chem. C, 4 (2016) 1704.
8. R. Cao, G. Chen, X. Yu, P. Tang, Z. Luo, S. Guo, G. Zheng, Enhanced photoluminescence of $CaTiO_3$:Sm^{3+} red phosphors by Na^+, H_3BO_3 added. Mater. Chem. Phys., 171 (2016) 222.
9. Q.L. Dai, M.E. Foley, C.J. Breshike, A. Lita, G.F. Strouse, Ligand-passivated Eu:Y_2O_3 nanocrystals as a phosphor for white light emitting diodes. J. Am. Chem. Soc., 133 (2011) 15475.
10. R.B. Basavaraj, H. Nagabhushana, G.P. Darshan, B. Daruka Prasad, M. Rahul, S.C. Sharma, R. Sudaramani, K.V. Archana, Red and green emitting CTAB assisted $CdSiO_3$:Tb^{3+}/Eu^{3+} nanopowders as fluorescent labeling agents used in forensic and display applications, Dyes Pigm., 147 (2017) 364.
11. G.P. Darshan, H.B. Premkumar, H. Nagabhushana, S.C. Sharma, B. Daruka Prasad, S.C. Prashantha, R.B. Basavaraj, Superstructures of doped yttrium aluminates for luminescent and advanced forensic investigations, J. Alloys Compd., 686 (2016) 577.
12. R.B. Basavaraj, H. Nagabhushana, G.P. Darshan, B. Daruka Prasad, S.C. Sharma, K.N. Venkatachalaiah, Ultrasound assisted rare earth doped Wollastonite nanopowders: Labelling agent for imaging eccrine latent fingerprints and cheiloscopy applications, J. Ind. Eng. Chem., 51 (2017) 90.
13. B.S. Rohini, H. Nagabhushana, G.P. Darshan, R.B. Basavaraj, S.C. Sharma, P. Amudha, M. Rahul, B. Daruka Prasad, Multifunctional applications of self - Assembled 3D CeO_2: Cr^{3+} hierarchical structures synthesized via ultrasound assisted sonochemical route, J. Alloys Compd., 724 (2017) 897.
14. G.S. Sodhi, J. Kaur, Powder method for detecting LFPs: A review, Forensic Sci. Int., 120 (2001) 172.

15. M. Venkataravanappa, R.B. Basavaraj, G.P. Darshan, B. Daruka Prasad, S.C. Sharma, P. Hema Prabha, S. Ramani, H. Nagabhushana, Multifunctional Dy (III) doped di-calcium silicate array for boosting display and forensic applications, J. Rare Earths, https://doi.org/10.1016/j.jallcom.2017.07.054.
16. G.S. Rama Raju, J.Y. Park, G.P. Nagaraju, E. Pavitra, H.K. Yang, B.K. Moon, J.S. Yu, Y.S. Huh, J.H. Jeong, Evolution of $CaGd2ZnO_5:Eu^{3+}$ nanostructures for rapid visualization of latent fingerprints, J. Mater. Chem. C, 5 (2017) 4246.
17. A. Sandhyarani, M.K. Kokila, G.P. Darshan, R.B. Basavaraj, B. Daruka Prasad, S.C. Sharma, T.K.S. Lakshmi, H. Nagabhushana, Versatile core-shell $SiO_2@SrTiO_3:Eu^{3+}$, Li^+ nanopowders as fluorescent label for the visualization of latent fingerprints and anti-counterfeiting applications, Chem. Eng. J., 327 (2017) 1135.
18. K.N. Venkatachalaiah, H. Nagabhushana, G.P. Darshan, R.B. Basavaraj, B. Daruka Prasad, Novel and highly efficient red luminescent sensor based $SiO_2@Y_2O_3:Eu^{3+}$, M^+ (M^+ = Li, Na, K) composite core–shell fluorescent markers for latent fingerprint recognition, security ink and solid state lightning applications, Sens. and Act. B: Chem., 251 (2017) 310.
19. H. Chen, R. Ma, Y. Chen, L. Fan, Fluorescence Development of Latent Fingerprint with Conjugated Polymer Nanoparticles in Aqueous Colloidal Solution, ACS Appl. Mater. Interfaces, 9 (2017) 4908.
20. S.J. Park, J.Y. Kim, J.H. Yim, N.Y. Kim, C.H. Lee, S.J. Yang, H.K. Yang, The effective fingerprint detection application using $Gd_2Ti_2O_7:Eu^{3+}$ nanophosphors, J. Alloys Compd., https://doi.org/10.1016/j.jallcom.2018.01.116.
21. G.S. Sodhi, J. Kaur, Powder method for detecting LFPs: A review, Forensic Sci. Int., 120 (2001) 172.
22. C. Lo, J. Duh, B. Chiou, C. Peng, L. Ozawa, Synthesis of Eu^{3+}-activated yttrium oxysulfide red phosphor by flux fusion method. Mater. Chem. Phys., 71 (2001) 179.
23. H.S. Kang, Y.C. Kang, K.Y. Jung, S.B. Park, Eu-doped barium strontium silicate phosphor particles prepared from spray solution containing NH_4Cl flux by spray pyrolysis. Mater. Sci. Eng. B, 121 (2005) 81.
24. Subhash Sharma, R. K. Dwivedi, Substitutionally driven phase transition and enhanced multiferroic and electrical properties of $(1-x)\ BiFeO_{3-(x)}\ Pb(Zr_{0.52}Ti_{0.48})O_3$ ceramics ($0.0 \leq x \leq 1.00$), J. Alloys Compd., 692 (2017) 770.
25. Subhash Sharma, Vikash Singh, R. K. Dwivedi, Rajeev Ranjan, Avneesh Anshul, S. S. Amritphale, Navin Chandra, Phase transformation, improved ferroelectric and magnetic properties of (1x) $BiFeO_{3-x}Pb(Zr_{0.52}Ti_{0.48})O_3$ solid solutions, J. Applied Phys., 115 (2014) 224106.
26. Publication CIE no 17.4 (1987) International Lighting Vocabulary, Central Bureau of the Commission Internationale de L 'Eclairage, Vienna, Austria.
27. C.K Jorgensen, R. Reisfeld, Judd-Ofelt parameters and chemical bonding, J. Less Comm. Met., 93 (1983) 107.
28. B. R. Judd, Optical absorption intensities of rare-earth ions, Phys. Rev., 127 (1962) 750.
29. G.S. Ofelt, Intensities of crystal spectra of rare-earth ions, J. Chem. Phys., 37 (1962) 511.
30. J. Kai, L. Zhang, J. Lu, C. Xu, C. Cai, H. Lin, Triple-Mode Emission of Carbon Dots: Applications for Advanced Anti-Counterfeiting, Angew. Chem., 55 (2016) 1.
31. P. Kumar, J. Dwivedi, B. K. Gupta, Highly luminescent dual mode rare-earth nanorod assisted multi-stage excitable security ink for anti-counterfeiting applications, J. Mater. Chem. C, 2 (2014) 10468.

32. M. Dhanalakshmi, H. Nagabhushana, G.P. Darshan, B. Daruka Prasad, Ultrasound assisted sonochemically engineered effective red luminescent labelling agent for high resolution visualization of latent fingerprints, Mat. Res. Bull., 98 (2018) 250.
33. G. P. Darshan, H. B. Premkumar, H. Nagabhushana, S. C. Sharma, S. C. Prashanth, B. Daruka Prasad, Effective fingerprint recognition technique using doped yttrium aluminate nano phosphor material, J. coll. inter. Sci., 464 (2016) 206.
34. G. P. Darshan, H. B. Premkumar, H. Nagabhushana, S. C. Sharma, B. Daruka Prasad, S. C. Prashantha, Neodymium doped yttrium aluminate synthesis and optical properties–A blue light emitting nanophosphor and its use in advanced forensic analysis, Dyes Pigm., 134 (2016) 227.
35. K. N. Venkatachalaiah, H. Nagabhushana, G. P. Darshan, R. B. Basavaraj, B. Daruka Prasad, S. C. Sharma, Blue light emitting Y_2O_3:Tm^{3+} nanophosphors with tunable morphology obtained by bio-surfactant assisted sonochemical route, Spectrochim. Acta Part A: Mol. and Biomol. Spect., 184 (2017) 89.
36. G. P. Darshan, H. B. Premkumar, H. Nagabhushana, S. C. Sharma, S. C. Prashantha, H. P. Nagaswarup, B. Daruka Prasad, Blue light emitting ceramic nano-pigments of Tm^{3+} doped $YAlO_3$: Applications in latent finger print, anti-counterfeiting and porcelain stoneware, Dyes Pigm., 131 (2016) 268.
37. S. Q. Xu, L. Z. Sun, Y. Zhang, H. D. Ju, S. L. Zhao, D. G. Deng, H.P. Wang, B. L. Wang, Effect of fluxes on structure and luminescence properties of $Y_3Al_5O_{12}$:Ce^{3+} phosphors, J. Rare Earths, 27(2009) 329.
38. L. H. Cheng, H. Y. Zhong, J. S. Sun, X. Q. Zhang, Y. Peng, T. Yu, X.X. Zhao, Flux and concentration effect on Eu^{3+} doped $Gd_2(MoO_4)_3$ phosphor, J. Rare Earths, 26 (2008) 214.

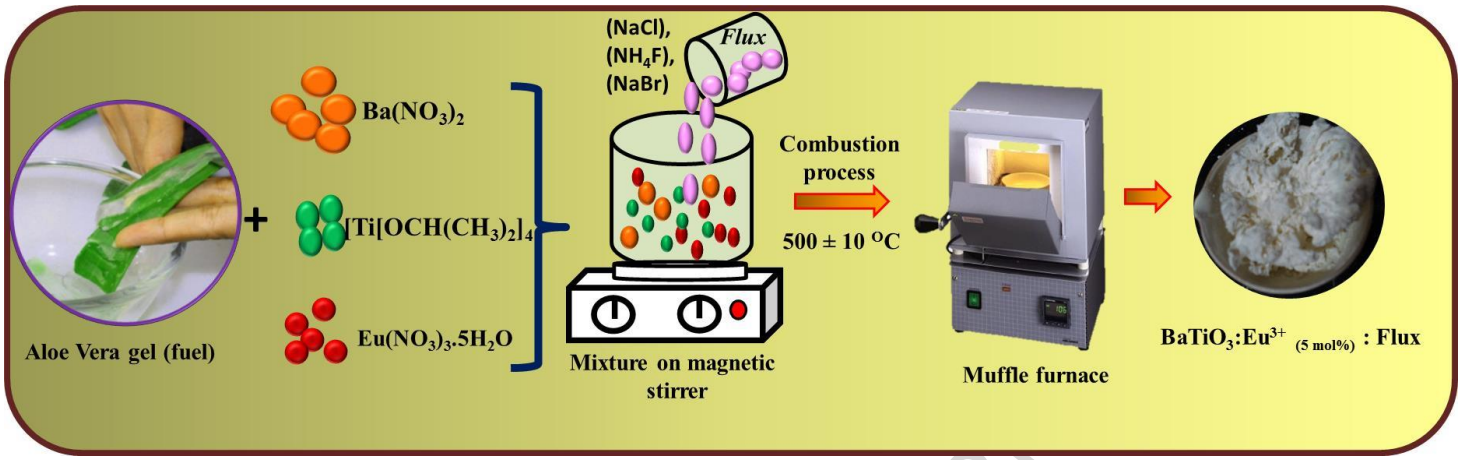

Fig.1. Schematic illustration of SC synthesis of $BaTiO_3:Eu^{3+}$ (5 mol %) NPs.

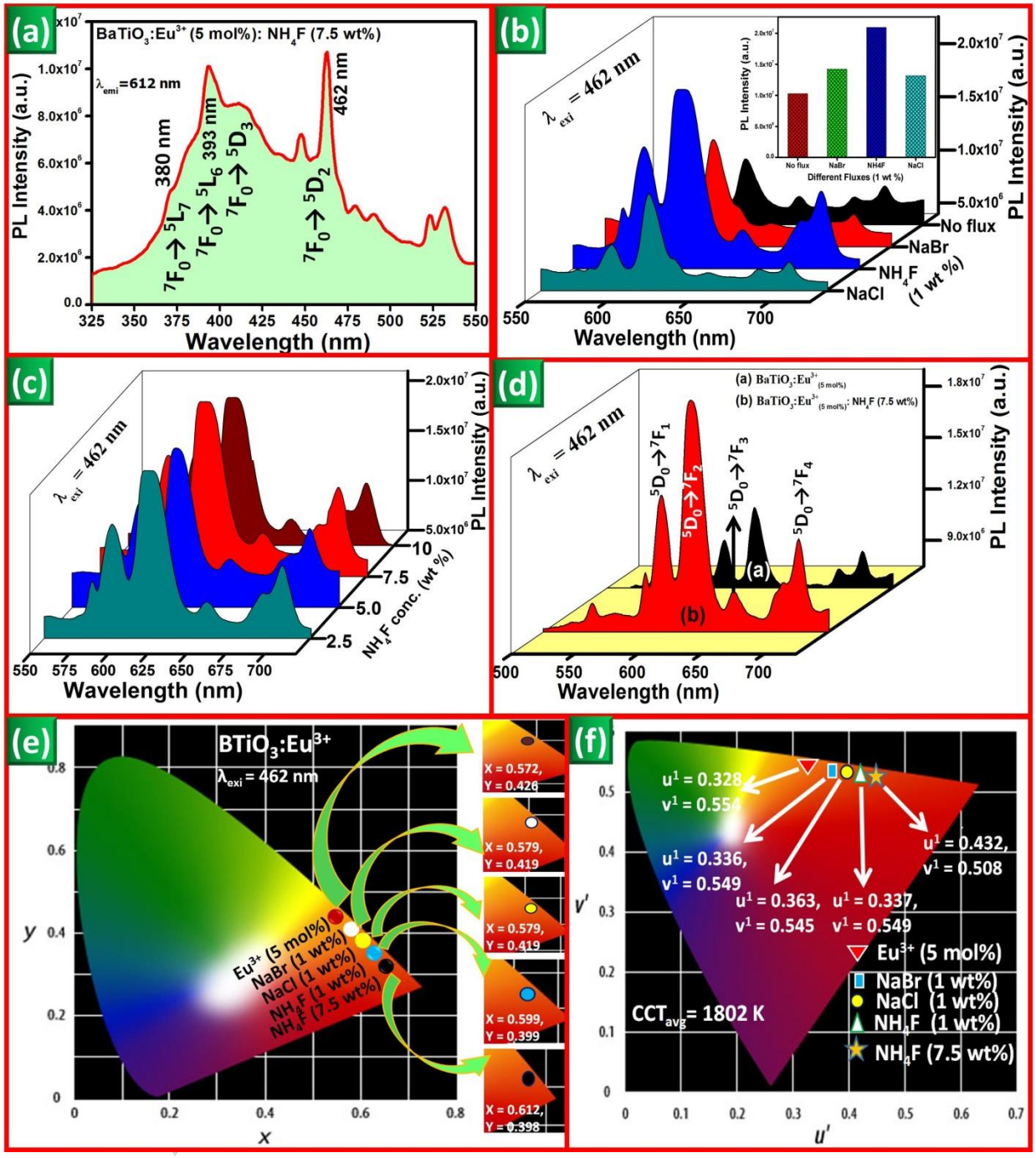

Fig.2 (a) Excitation spectrum of $BaTiO_3:Eu^{3+}$ (5 mol %): NH_4F (7.5 wt %) NPs, (b) PL emission spectra of $BaTiO_3:Eu^{3+}$ (5 mol %) NPs with various fluxes (Inset: PL Intensity v/s various fluxes), (c) emission spectra of $BaTiO_3:Eu^{3+}$ (5 mol %) with NH_4F (2.5, 5, 7.5, 10 wt %) NPs, (d) emission spectra of $BaTiO_3:Eu^{3+}$ (5 mol %) and BENF NPs, (e) CIE and (f) CCT diagrams of $BaTiO_3:Eu^{3+}$ (5 mol %) NPs with and without fluxes.

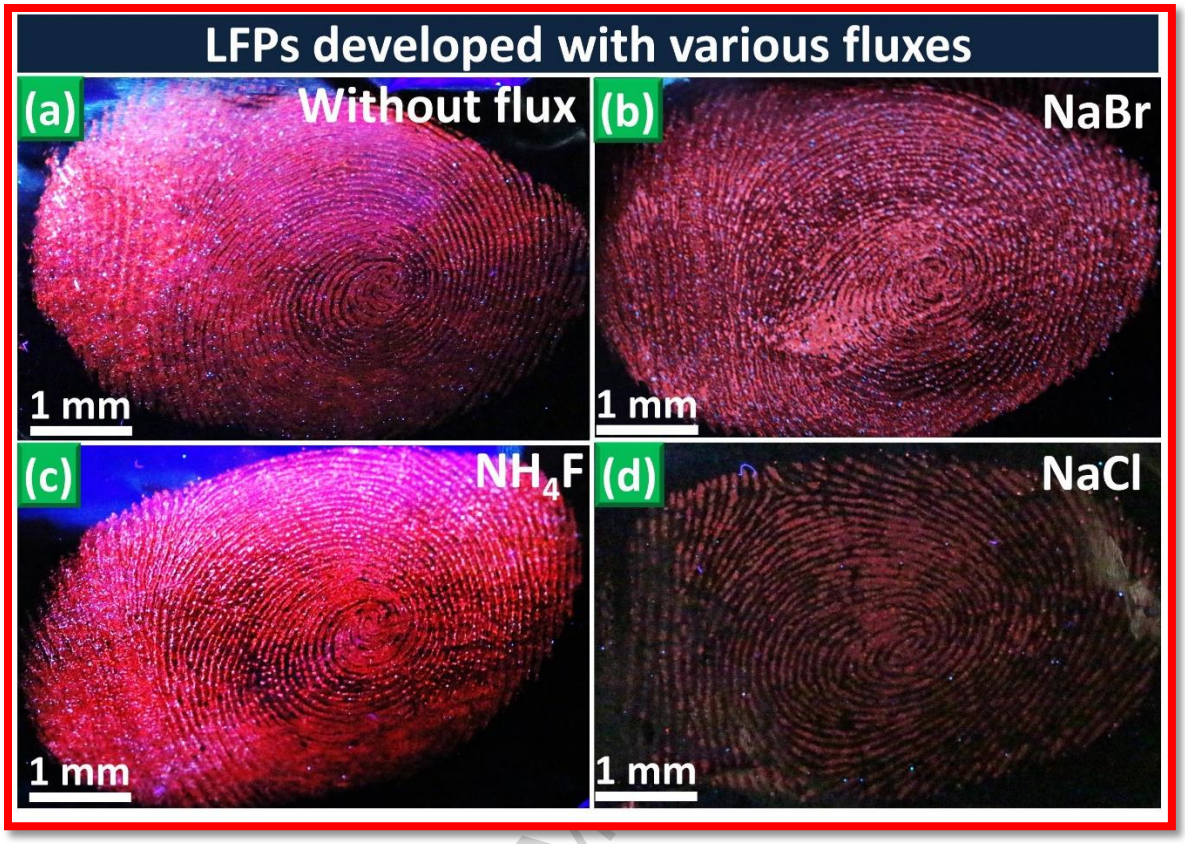

Fig.3. LFPs visualized on aluminum foil surface stained by $BaTiO_3:Eu^{3+}$ (5 mol %) NPs with and without fluxes.

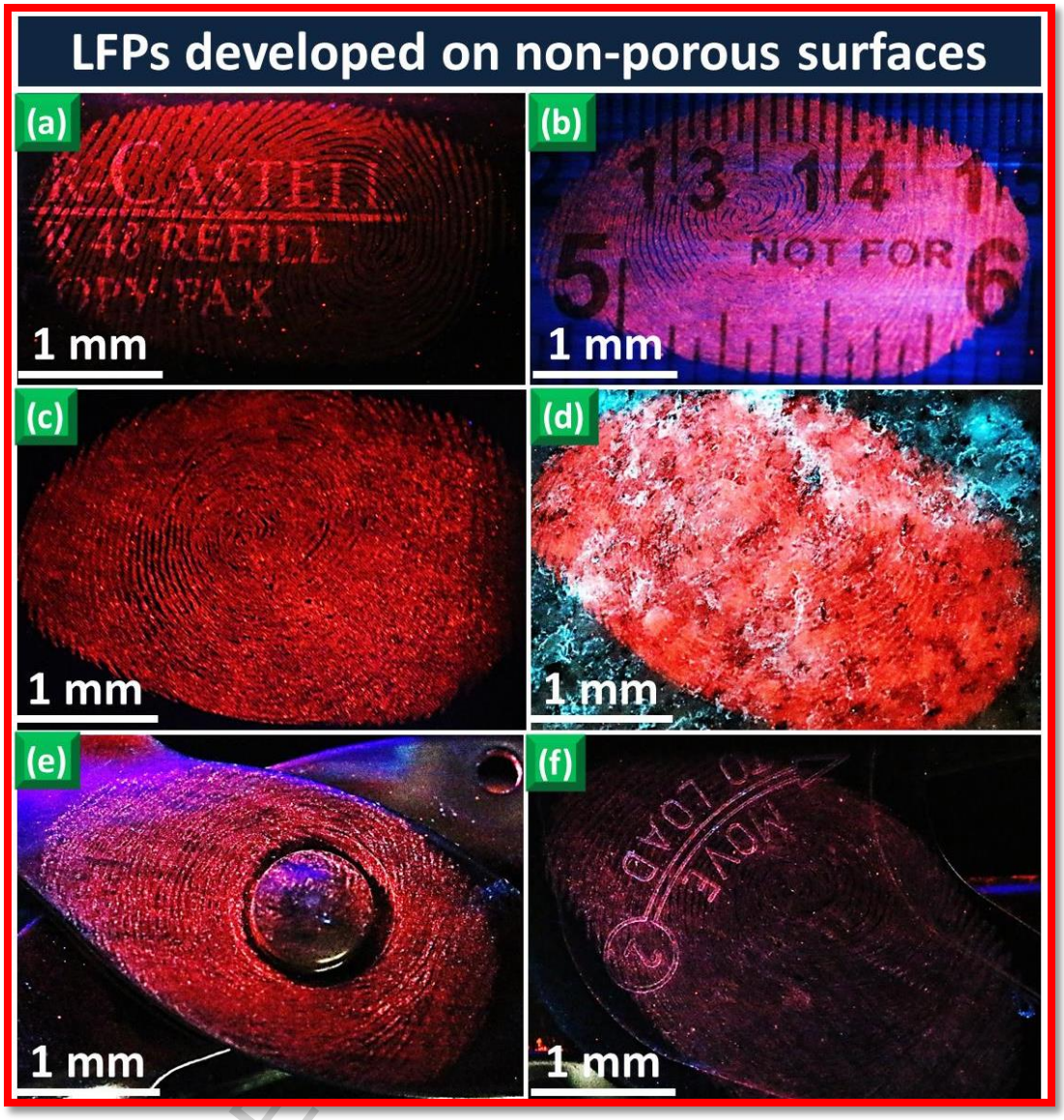

Fig.4. LFPs visualized on various non-porous surfaces stained by using optimized BENF NPs under UV 254 nm light irradiation.

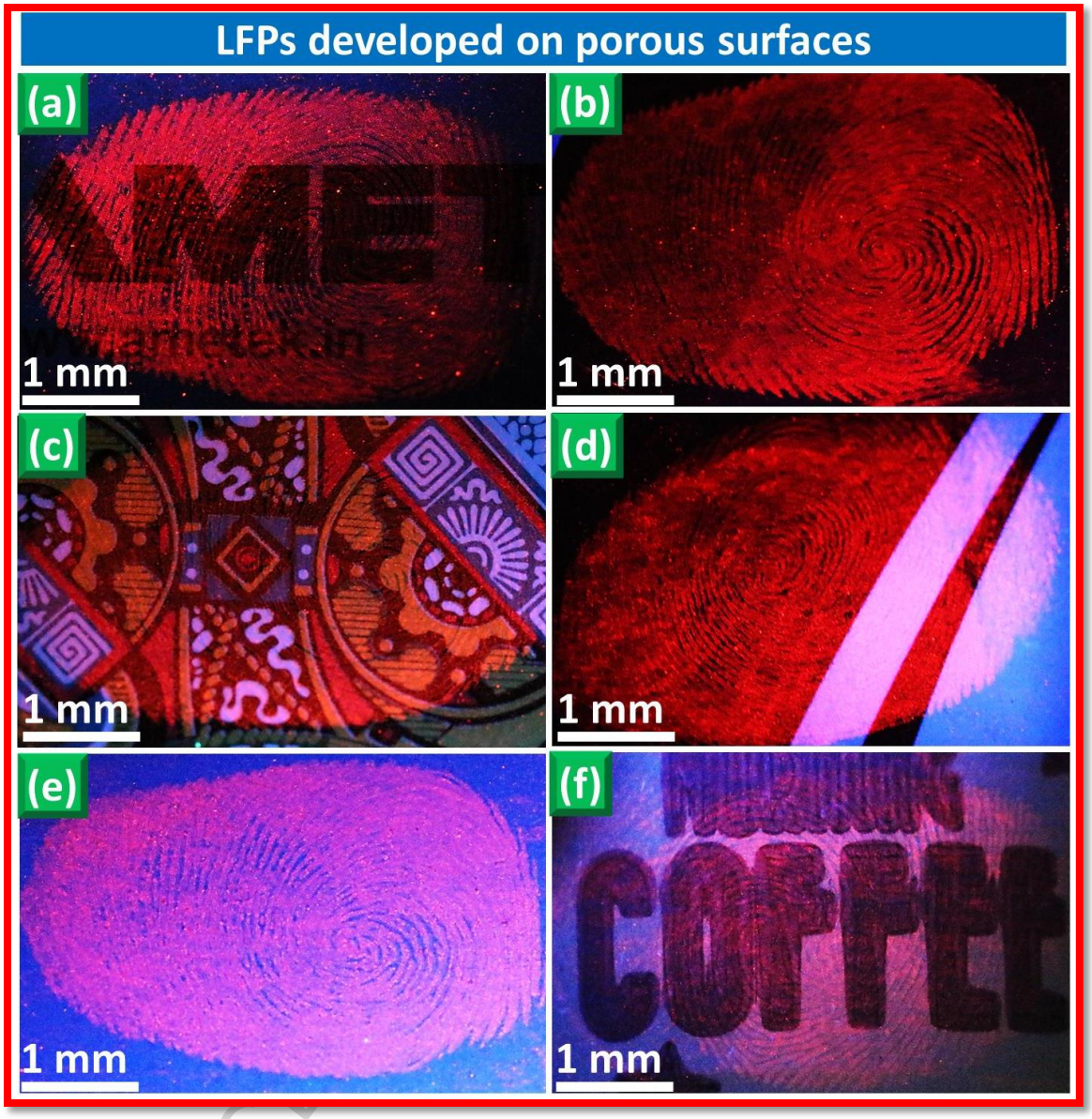

Fig.5. Visualized LFPs on various porous surfaces with different background using optimized BENF NPs under UV 254 nm light irradiation followed by powder dusting technique.

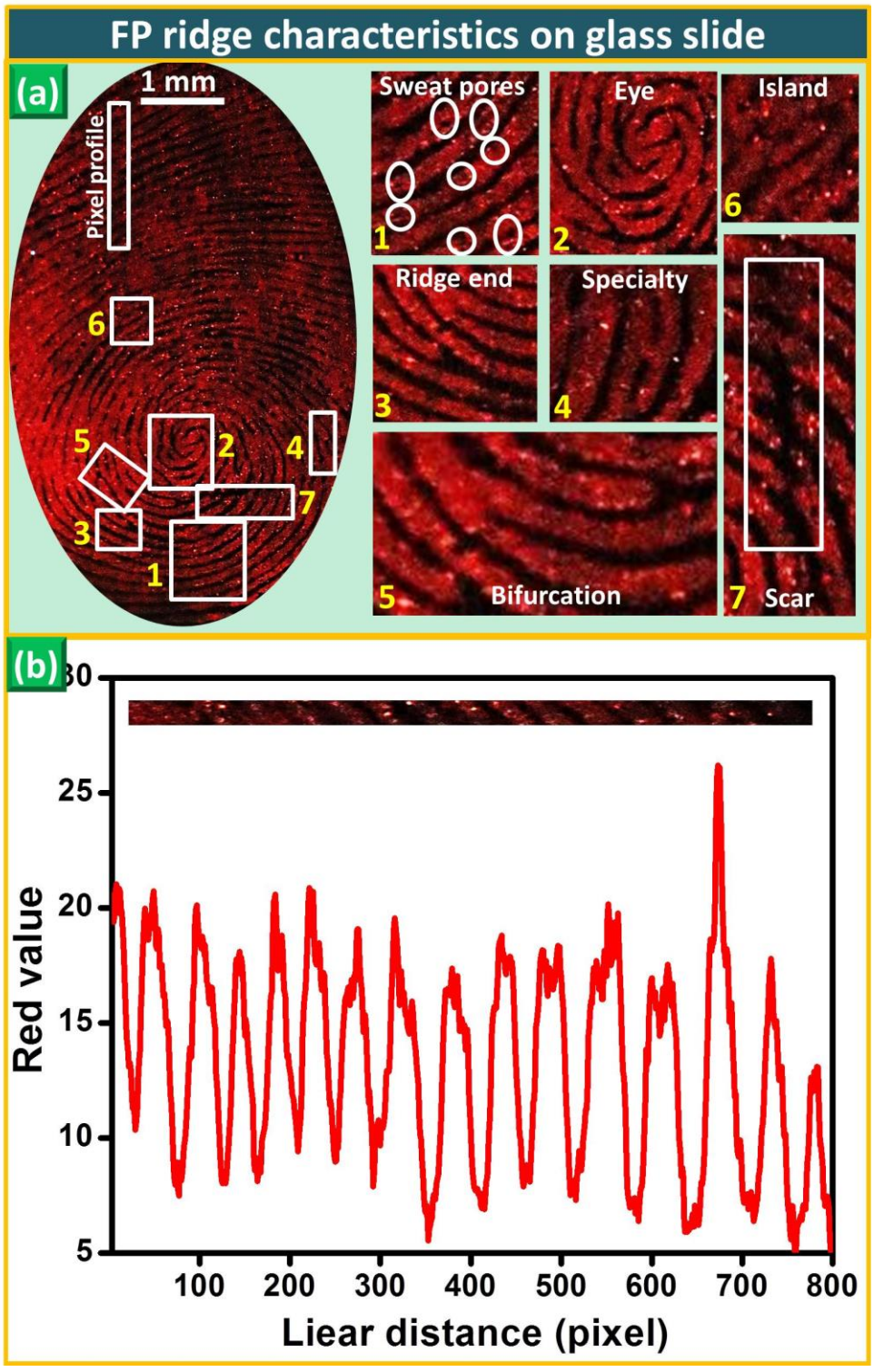

Fig.6 (a) Various FP ridge characteristics on glass slide stained by using optimized BENF NPs under UV 254 nm light and (b) pixel profile showing the fluctuation of red value with ridge (red) and furrow (black) over a few papillary ridges indicated by rectangle box (Fig.6 (a)).

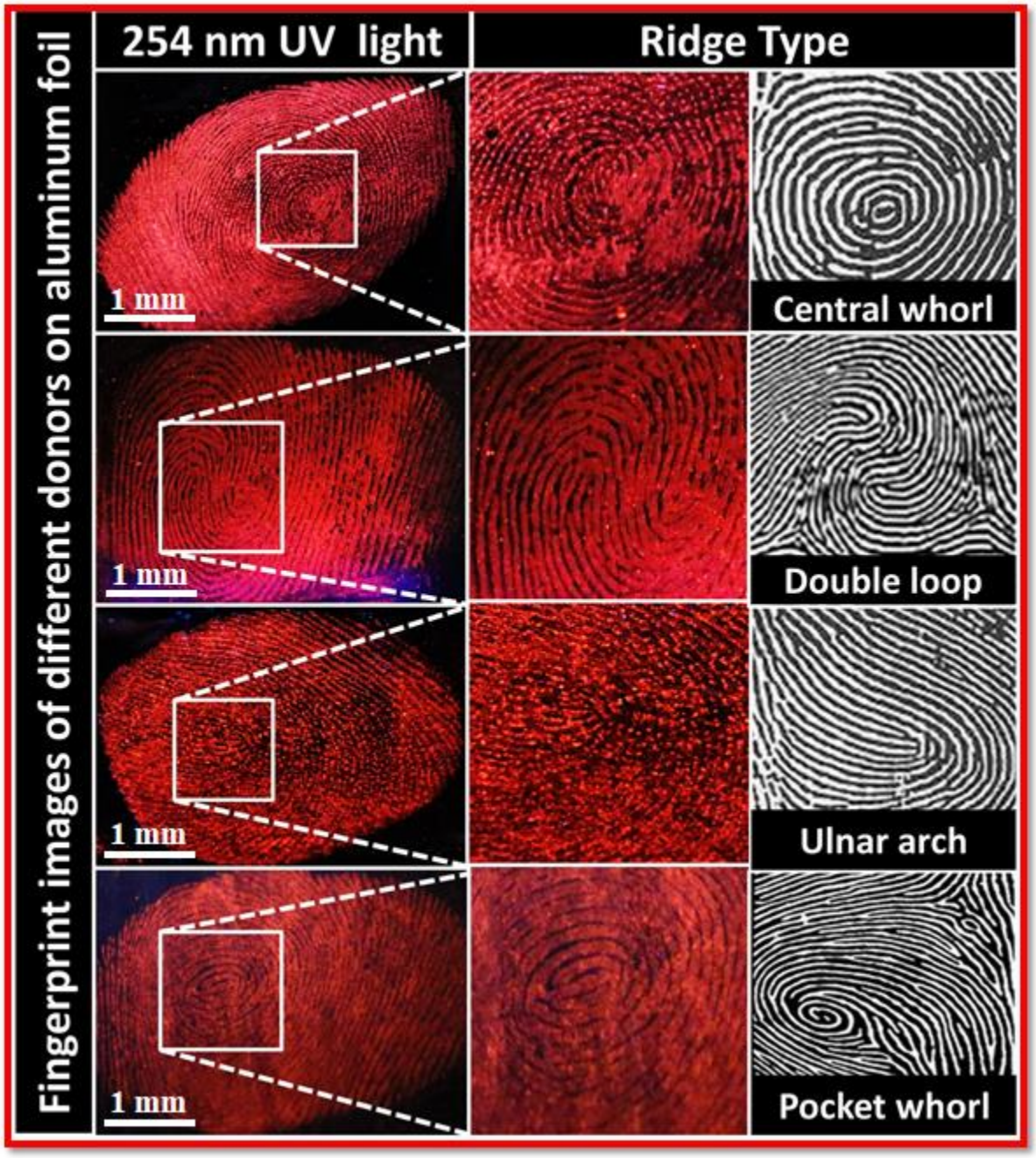

Fig.7. Visualization of LFPs of different donors on aluminum foil surface under UV 254 nm light.

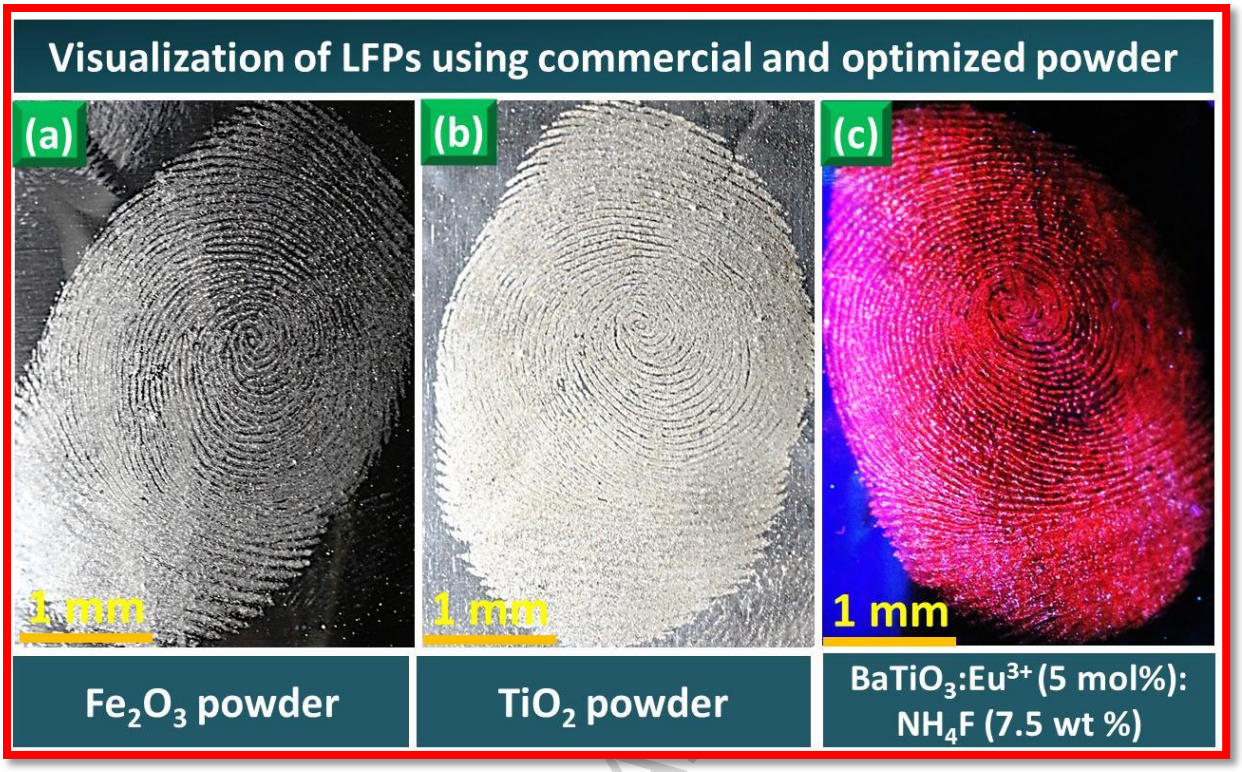

Fig.8. Comparison of visualized LFPs stained using commercial powders and optimized BENF NPs on aluminum foil surface.

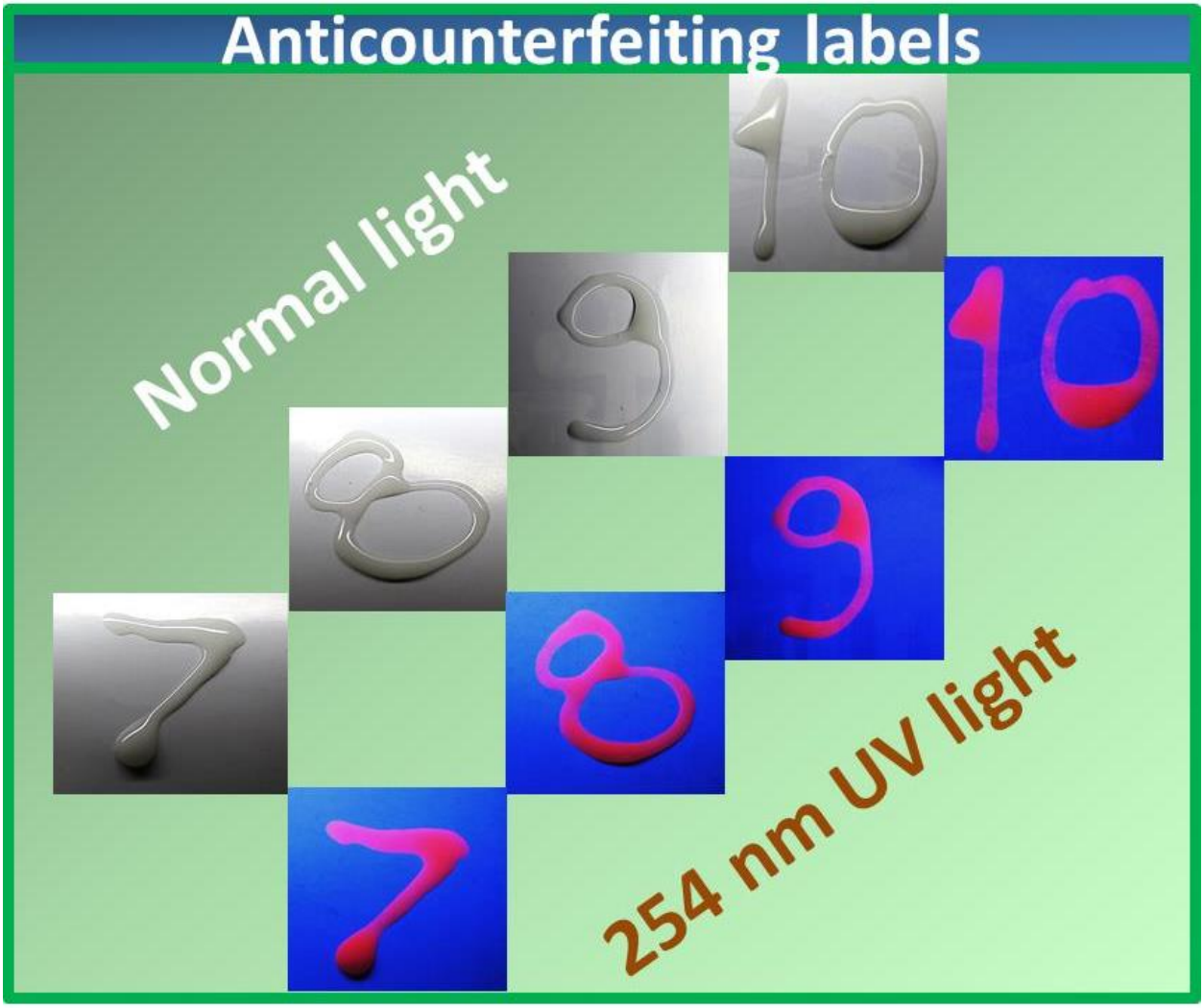

Fig.9. AC labels prepared using optimized BENF NPs based ink under normal and UV 254 nm light.

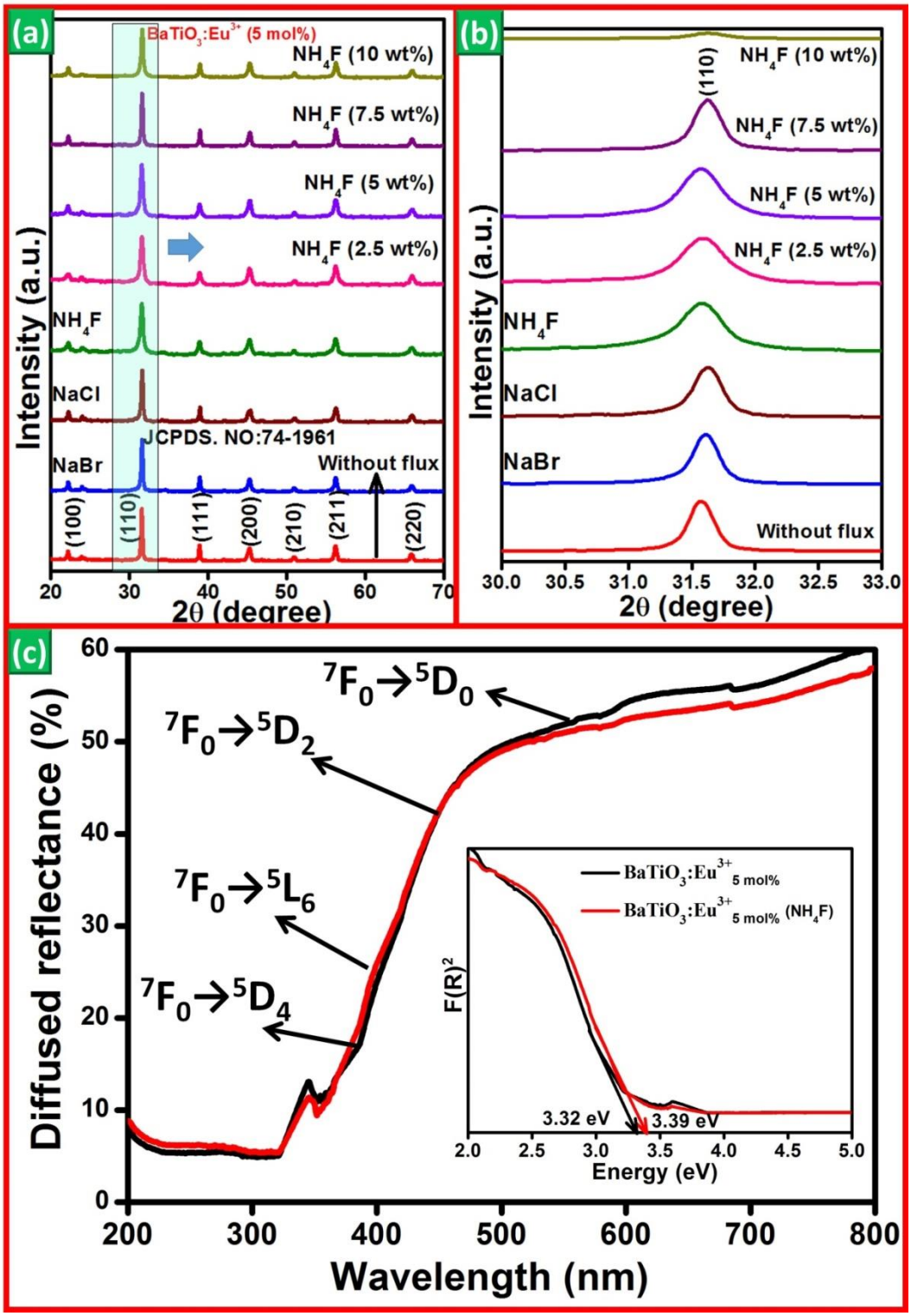

Fig.10 (a) PXRD patterns of $BaTiO_3:Eu^{3+}$ (5 mol %) with and without fluxes, (b) magnified view of peak (110) and (c) DR spectra of $BaTiO_3:Eu^{3+}$ (5 mol %) and $BaTiO_3:Eu^{3+}$ (5 mol %): NH_4F (1 wt %) (Inset: energy band gap plot).

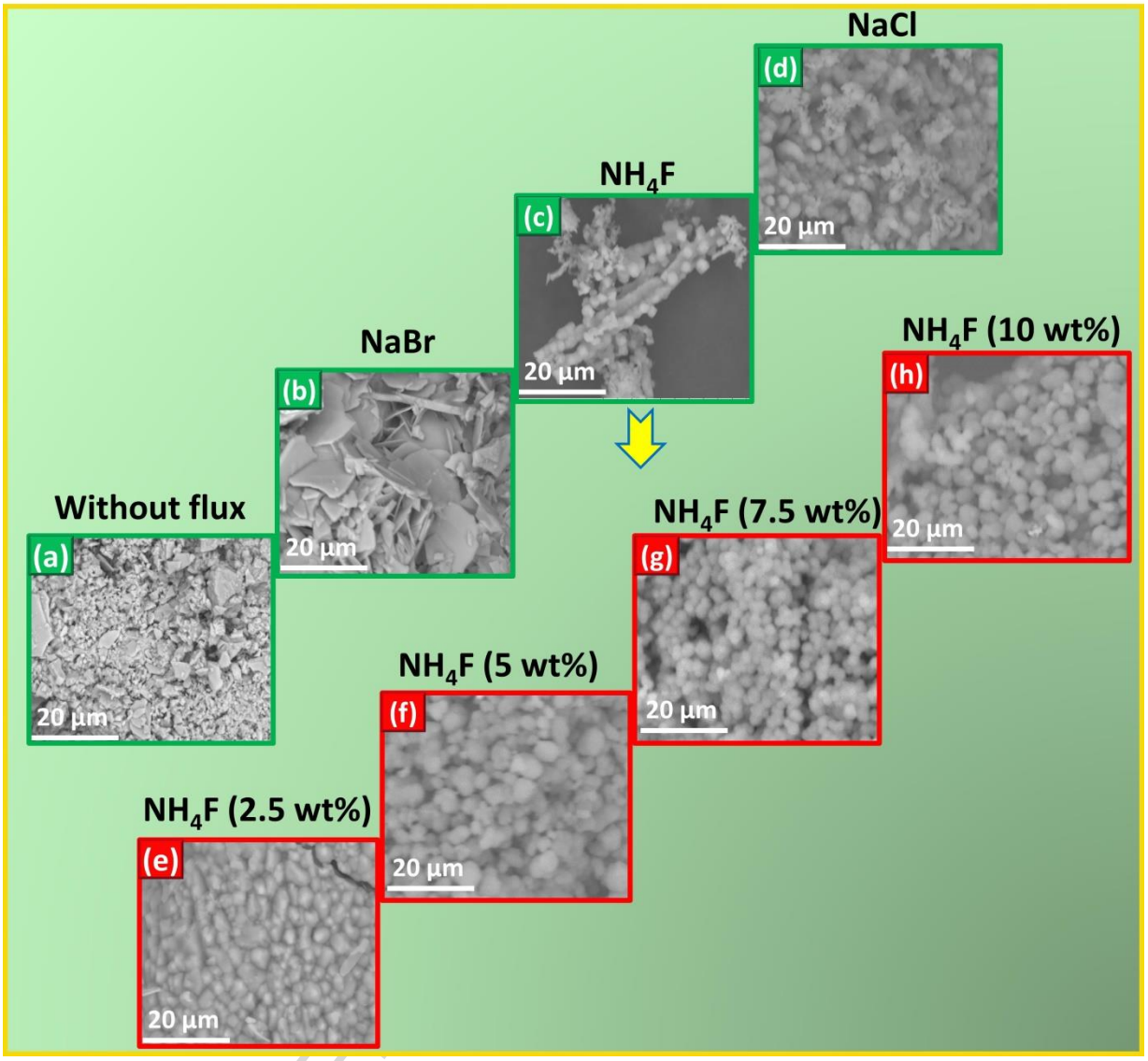

Fig.11. SEM micrographs of (a-d) $BaTiO_3:Eu^{3+}$ (5 mol %) with and without fluxes and (e-h) $BaTiO_3:Eu^{3+}$ (5 mol %): NH_4F (2.5, 5, 7.5, 10 wt %) NPs.

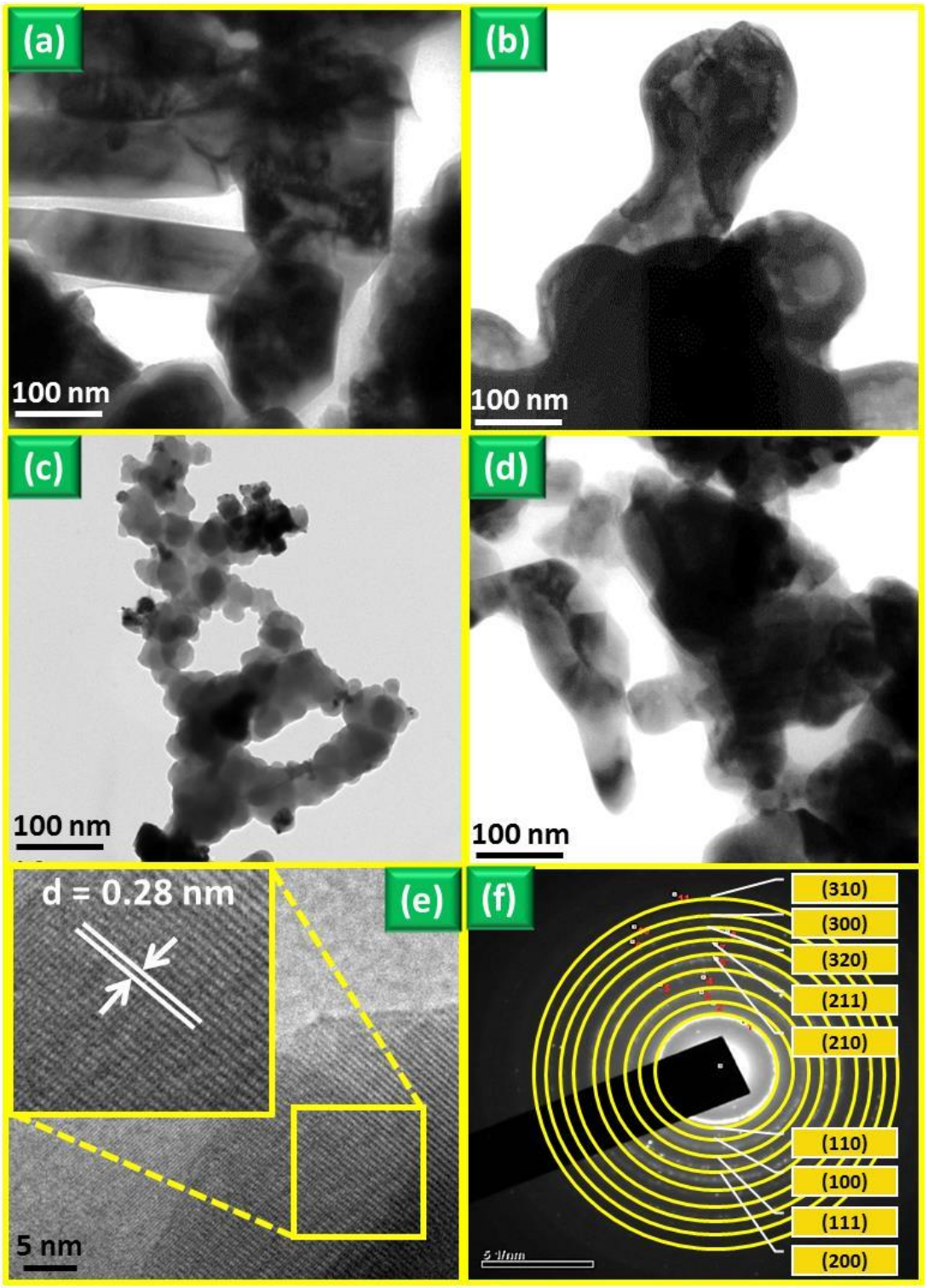

Fig.12. TEM image of $BaTiO_3:Eu^{3+}$ (5 mol %) NPs (a) without flux and with (b) NaBr, (c) NH_4F, (d) NaCl, (e & f) HRTEM image and SAED patterns of optimized BENF NPs.

Table.1. J-O intensity parameters (Ω_2 & Ω_4), branching ratio (β_R), calculated radiative (τ_{rad}) lifetime, asymmetric ratio (A_{21}), radiative transition probability (A_T) and quantum efficiency (η) of $BaTiO_3:Eu^{3+}$ (5 mol %) NPs with and without fluxes.

Flux (1 wt %)	**Judd-Ofelt intensity parameters ($\times 10^{-20}$ cm^{-1})**		**β_{calc}**	**τ_{rad} (ms)**	**A_{21}**	**A_T (s^{-1})**	**η (%)**
	Ω_2	**Ω_4**					
No flux	3.79	5.87	0.066	1.32	2.34	756	75.09
NaBr	1.64	2.62	0.093	1.87	1.01	311	77.05
NaCl	1.40	2.22	0.140	2.80	1.02	356	76.62
NH_4F	1.24	1.38	0.160	3.20	1.45	532	89.66

Research Highlights

- Fluxes blended $BaTiO_3:Eu^{3+}$ (5 mol %) NPs were prepared by combustion route.
- The optimized sample was used as a sensing agent for visualization of LFPs.
- High sensitivity, selectivity and little background hindrance FPs were revealed.
- The optimized product was used for forensic and WLED's applications.